XIV. GASEOUS ELECTRONICS*

Academic and Research Staff

Prof. E. V. George
Prof. G. Bekefi
Prof. S. C. Brown
Dr. C. K. Rhodes
J. J. McCarthy
W. J. Mulligan

Graduate Students

W. J. Amisial
J. L. Miller
C. W. Werner
D. Wildman

RESEARCH OBJECTIVES AND SUMMARY OF RESEARCH

1. Plasma Physics of Gaseous Lasers

Our general objectives are concerned with a study of the plasma physics of gaseous lasers. We have found that to obtain high peak laser output power from a high-pressure CO_2 laser system the electrical energy should be delivered to the lasing media in a very short time, of the order of ~100 ns. Part of our effort is devoted to understanding the mechanisms that limit the rapid transfer of electrical energy into a high-pressure gas.

Recently, researchers in this country and in the Soviet Union have obtained stimulated emission in xenon at a wavelength of ~1700 Å. We are studying the feasibility of exciting such systems in a CO_2 laser-produced plasma.

E. V. George

2. Plasma Physics Information Retrieval

The cyclic character of research interests has been noted many times and one of the best examples of it is found in the field of gaseous electronics. Thirty years ago, and even up to 10 years ago, the study of the details of electrical discharges in gases was a field of pure physics which seemed to have little practical application, although it was interesting in terms of energy distribution functions and charged-particle collision kinetics. With the emergence of tremendous interest in gas-discharge lasers, the fundamental studies have suddenly become of such vital interest to all research workers in the field of gas lasers that the great task now is to apply 30 years of familiarity with the field to a multitude of problems arising daily in the laboratory as new lasers are discovered and new gas mixtures are tried and perfected. My primary work in the Gaseous Electronics Group centers around the application of fundamental gas discharge physics to laser production and the interaction of high-power laser pulses with low-density plasmas.

The specific mechanisms of energy transfer in both CO and CO_2 laser systems are still not understood, but are under active study as are the gas discharge mechanisms in high-pressure noble gases of interest in ultraviolet lasers.

---

*This work is supported by the Joint Services Electronics Programs (U.S. Army, U.S. Navy, U.S. Air Force) under Contract DAAB07-71-C-0300 and by the University of California, Lawrence Livermore Laboratory, Livermore (Subcontract No. 7877409).

In addition to applying the classical concepts of gas discharge physics to our current laboratory laser problems, I am engaged in the difficult problem of keeping the laboratory up-to-date with greatly proliferating research literature. In 1958, with Professor W. P. Allis, I published Technical Report 283 (Fourth Edition), entitled "Basic Data of Electrical Discharges," in the R. L. E. series. This proved so useful that almost immediately I started a more ambitious attempt to make the basic data of the field available, which culminated in Special Technical Report Number 2 of the Research Laboratory of Electronics, which was published in August 1959, in a book, entitled Basic Data of Plasma Physics (336 p.). These reports had been assembled by hand from abstract journals, but by mid 1960 with the beginning of a real push to gaseous electronics from the gas laser field, it became clear that computer retrieval was the only practical solution, and in cooperation with Project TIP I experimented with computerization of data searching and another Basic Data of Plasma Physics was published by The M. I. T. Press, Cambridge, Mass., 1966.

With the demise of the IBM 7094 computer and the transfer of the TIP literature input to the American Institute of Physics, in New York, the particular computer programs for literature searching came to an end at the Research Laboratory of Electronics.

A fair number of new literature retrieval schemes have been inaugurated, and using the experience I have had with this kind of retrieval aimed specifically at the gaseous electronics field, I am now trying to devise a current literature-awareness technique specifically applicable to our study of the plasma physics of gaseous lasers. My hope, in the long run, is to develop a system that will not require a major commitment of time from a member of the senior staff, but can still provide necessary information and data from the ever-expanding "literature explosion."

S. C. Brown

A. STIMULATED ULTRAVIOLET EMISSION FROM A PLASMA

Joint Services Electronics Programs (Contract DAAB07-71-C-0300)

E. V. George, C. K. Rhodes

[Dr. C. K. Rhodes is supported under the auspices of the U. S. Atomic Energy Commission. His permanent address is: Department of Physics, Lawrence Livermore Laboratory, Livermore, California]

Recent developments in this country and in the Soviet Union indicate that the noble gases can be used as a medium for high-power laser systems in the vacuum ultraviolet wavelength region. We show that it may be possible to excite such a system in a conventional discharge, in a laser-produced plasma, or with relativistic beams.

1. Introduction

The ultraviolet continua of excited rare gas systems have been known for many decades.[1] These continuum emissions have been examined more recently[2] and have found application as convenient light sources covering essentially the entire vacuum ultraviolet for wavelengths longer than approximately 1000 Å. The continuous radiations originate from bound-free transitions of molecular dimers, such as Ar_2, Kr_2, or Xe_2. In typical cases of interest the excited state is characterized by a potential function $V^*(R)$ that

has a substantial potential minimum at an internuclear separation R_o and supports several vibrational levels. In contrast, the ground-state interatomic potential V(R) is generally strongly repulsive for $R \sim R_o$, although it does exhibit a relatively shallow van der Waals minimum at internuclear distances substantially greater than R_o. Figure XIV-1 illustrates these potential curves schematically. It is characteristic that the triplet state lies somewhat below the singlet level because of exchange. Data on He_2 and Xe_2 have been reported more completely than on others, although there are still large uncertainties in the precise location of many of the potential curves even in these cases.[3] The complex nature of these molecular systems is immediately recognized, since more than 60 electronic states are now known for even the simplest system He_2^*.

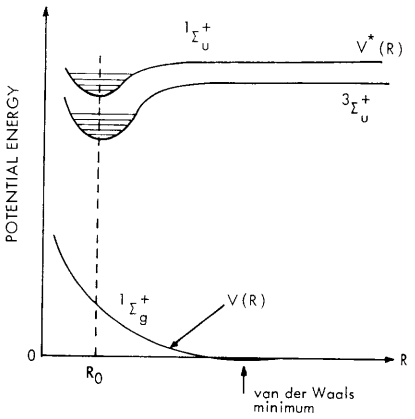

Fig. XIV-1.

Potential energy vs internuclear separation (R) for ground state (V(R)) and typical lowest excited molecular states ($V^*(R)$).

To a very good approximation, these excited molecular dimers can be regarded as Rydberg states. In this view the molecular configurations are then composed of two parts: the molecular ion core $\left(He_2^+\right)$ and a single excited electron orbiting largely outside of the region occupied by the core. We then have a relatively simple Rydberg series[4] which is characteristic of that core state. This model predicts that the equilibrium internuclear separation R_o, the molecular vibrational frequency, and the molecular moment of inertia are determined largely by the corresponding properties of the molecular ionic core. The potential curves for He_2^* given by Ginter and Battino[3] quite strikingly indicate the validity of this approximate model. It would appear that this feature introduces a very desirable simplification into an otherwise rather complicated situation, since it should be possible to formulate meaningful estimates of matrix elements on the basis of an essentially one-electron case.

An interesting property of these systems derives from the fact that certain continuous bands are observed with very similar characteristics in all three phases, gas, liquid, and solid. For example, the argon continuum centered near 1300 Å resulting from excitation by Americium α-particles exhibits essentially identical line shapes

(within ~10%) for all three phases.[5] Therefore we are strongly motivated to conclude that the excited species in all cases very closely resemble the gaseous dimer which is only negligibly influenced by the weak van der Waals forces of the surrounding neighbors in the liquid and solid phases. This suggests the possibility that these systems may be successfully operated at liquid or solid density.

Recently, H. A. Koehler et al.,[6] at Lawrence Livermore Laboratory, obtained stimulated ultraviolet emission from gaseous xenon at pressures above 200 psi. In their experiments xenon was excited by a high current density, relativistic electron beam. The gas was placed in an optical cavity and the stimulated emission occurred at a wavelength of 1716 Å. By studying the temporal characteristics of the spontaneous emission, they concluded that the radiative lifetime of the excited xenon dimer is short, with a value of ~20 ns. Further studies of the vacuum ultraviolet emission from rare gas mixtures excited with relativistic electron beams have been made by Krawetz and Rhodes.[7]

2. Basic Processes Operative in the Rare Gas Molecular Systems

We shall now discuss the various kinetic processes that lead to the formation of excited dimers. We illustrate some of these processes by means of Xe. It is important, however, to note that the various rates for all of these reactions are not known at this time.

$$e + Xe \rightarrow e + Xe^* \quad (1)$$

$$e + Xe \rightarrow e + e + Xe^+ \quad (2)$$

$$e + Xe^* \rightarrow e + e + Xe^+ \quad (3)$$

$$Xe^* + Xe^* \rightarrow Xe^+ + e + Xe \quad (4)$$

$$Xe^* + Xe \rightarrow Xe_2^+ + e \quad (5)$$

$$Xe^* + Xe + Xe \rightarrow Xe_2^* + Xe \quad (6)$$

$$Xe^+ + Xe + Xe \rightarrow Xe_2^+ + Xe \quad (7)$$

$$Xe_2^* + Xe_2^* \rightarrow Xe_2^+ + e + Xe + Xe \quad (8)$$

$$\gamma + Xe_2^* \rightarrow Xe_2^+ + e \quad (9)$$

$$Xe_2^+ + e \rightarrow Xe^* + Xe \quad (10)$$

$$Xe_2^* \rightarrow \gamma + Xe + Xe \quad (11)$$

$$Xe^{**} + Xe \rightarrow Xe^* + Xe \quad (12)$$

$$Xe^{**} + e \rightarrow Xe^* + e \quad (13)$$

$$Xe_2^*(v) + Xe \rightarrow Xe_2^*(v') + Xe \quad (14)$$

Reactions (1) and (2) represent direct electron excitation and ionization by hot electrons. Data for reaction (1) are not available, but in helium the cross section for electron collisions promoting helium from the $1^1S \rightarrow 3^3P$ state has a maximum value of $\sim 7 \times 10^{-19}$ cm^2 at an electron energy[8] of ~40 eV. The cross section for (2) has a maximum value of $\sim 5 \times 10^{-15}$ cm^2 at an electron energy[9] of ~100 eV. The excited xenon atoms can be lost by collisions with low-energy electrons [reaction (3)]. These low-energy electrons can promote the excited xenon atom (initially, for example, in the ^3P manifold) to either a higher state of excitation or to the ionized state represented by reaction (3). For the case of argon, Wojaczek[10] has obtained a cross section of $\sim 10^{-15}$ cm^2 for this process. A large value might be anticipated because of the structural similarity of excited xenon and ground-state cesium. Reactions (4) and (8) illustrate the Penning ionization of both the excited atom and dimer states. Generally speaking, both processes represent a loss mechanism for these states. Although these cross sections are not available for the reactions illustrated above, the rate has been measured[11] for the process involving the helium metastable $He(2^3S_1)$:

$$He(2^3S_1) + He(2^3S_1) \rightarrow He^+(1^2S_{1/2}) + He(1^1S_o) + e.$$

The cross section was found to be $\sim 10^{-14}$ cm^2, which is a large value. Large values of these cross sections are not unexpected, since the excited states represent a significant charge expansion going to the next shell. The Hornbeck-Molnar process,[12] reaction (5), involves the collision of a highly excited xenon atom (excited state within ~1 eV from the ionization limit) with a ground-state xenon atom in a two-body process. Dahler et al.[13] have estimated this rate as $\sim 10^{-11}$ cm^3 s^{-1} for argon. These excited and ionized atoms will combine in three-body processes to form the corresponding molecule and molecular ion as given by reactions (6) and (7). The rate for process (6), excited dimer formation, has been found[14] to be $\beta \approx 2.5 \times 10^{-32}$ cm^6 s^{-1}. The rate for the formation of the molecular ion in a three-body process, reaction (6), is not known for xenon, although it is expected to be faster than 10^{-31} cm^6 s^{-1} on the basis of comparison with other known processes.[15] Connor et al.[16] estimate this rate to be $\beta_+ \gtrsim 10^{-31}$ cm^6 s^{-1} for neon. Since the lowest excited molecular state is more than half way

up from the molecular ground state to the convergence of the Rydberg series at the ground molecular ionic state. the continuum emission of the $^3\Sigma_u^+ \rightarrow {}^1\Sigma_g^+$ transition is sufficient to photoionize the $^3\Sigma_u^+$ state. This process [reaction (9)] will then be a stimulated loss, diminishing the optical gain on the $^3\Sigma_u^+ \rightarrow {}^1\Sigma_g^+$ transition. In order to estimate the photoionization cross section for the excited dimer, we shall make use of the fact that these excited dimers can be regarded as Rydberg states, that is, a molecular ion core $\left(Xe_2^+\right)$, and a single orbiting electron. The configuration of this orbiting electron is similar to the outer electron in ground-state cesium. In cesium[17] the photoionization cross section has been found to be $\sim 10^{-19}\ cm^2$. The dissociative recombination process (10) provides an effective channel to convert the ionized material into excited atomic species. We shall capitalize on this very fast process. The dissociative recombination coefficient for xenon[18] is $\alpha \sim 1.4 \times 10^{-6}\ cm^3\ s^{-1}$. Process (11) illustrates a spontaneous radiative bound-free transition of the molecular state corresponding, for example, to the $^3\Sigma_u^+ \rightarrow {}^1\Sigma_g^+$ transition shown in Fig. XIV-1. This transition is an allowed electric dipole process through strong spin-orbit coupling, as in the atom. Indeed, in the higher Z materials, such as Kr_2^* and Xe_2^*, it is anticipated that the spin selection rule is quite ineffective, as it is in the atomic case.[19] Although there has been disagreement regarding the spontaneous emission rate of Xe_2^*, ranging from 500 ns[14] to 20 ns,[6] recent experimental studies[6,7] clearly indicate that the shorter values are correct. Atomic and molecular relaxation processes are indicated in (12), (13), and (14). In the atomic case we want to collapse the manifold of excited states to the $^3P_2$ level which correlates with the lowest[3b] molecular excited state $\left({}^1S_o + {}^3P_2 \longleftrightarrow {}^3\Sigma_u^+\right)$. Both electrons and atoms can participate in these processes. Because of exchange, slow electrons can be very important, involving particularly magnetic transitions and transitions requiring a change in the electronic spin state. For instance, Phelps[20] had determined in neon the relaxation rates of $^3P_1 \rightarrow {}^3P_2$ through collisions with neon atoms and electrons. For the atomic collision partners the cross section is $\sim 10^{-19}\ cm^2$, while for the electrons the cross section is near the unitary bound for S-wave scattering with a value of $\sim 10^{-13}\ cm^2$. Molecular vibrational relaxation is illustrated as reaction (14). This may be a very efficient process requiring only a few gas kinetic collisions because of the possibility of resonant atom exchange.

For xenon some of the rates and cross sections for the processes discussed above are listed as follows.

$$Q \sim 10^{-15}\ cm^2 \qquad \text{(low-energy electrons)} \qquad (3)$$

$$Q \sim 10^{-14}\ cm^2 \qquad \text{(estimate)} \qquad (4)$$

$$\alpha \sim 10^{-11}\ cm^3\ s^{-1} \qquad \text{(estimate)} \qquad (5)$$

$$\beta \approx 2.5 \times 10^{-32}\ cm^6\ s^{-1} \qquad (6)$$

$$\beta_+ \approx 10^{-31}\ \text{cm}^6\ \text{s}^{-1} \qquad \text{(estimate)} \qquad (7)$$

$$Q \sim 10^{-14}\ \text{cm}^2 \qquad \text{(estimate)} \qquad (8)$$

$$Q \sim 10^{-19}\ \text{cm}^2 \qquad (9)$$

$$\alpha \approx 1.4 \times 10^{-6}\ \text{cm}^3\ \text{s}^{-1} \qquad (10)$$

$$\tau_{\text{spont}} \sim 20\ \text{ns} \qquad (11)$$

$$Q \sim 10^{-19}\ \text{cm}^2 \qquad (12)$$

$$Q \sim 10^{-13}\ \text{cm}^2 \qquad (13)$$

$$\alpha \sim 10^{-10}\ \text{cm}^3\ \text{s}^{-1} \qquad (14)$$

3. Plasma Model

Our major objective is to obtain stimulated ultraviolet emission from a gas without providing for relativistic electron-beam pumping. It must be emphasized that the characteristics of the plasma, formed by the passage of a relativistic electron beam through a high pressure gas, are not well known. It is known, however, that as this beam traverses the gas it produces secondary electrons (and ions). The velocity distribution (or energy distribution) is thought to be far from Maxwellian and calculations[21] indicate that the high-energy tail of the distribution is "rich" in electrons. We speculate from such data[21] that, on the average, the secondaries are hot, say ~10 eV or more. Moreover, these plasmas are generally not fully ionized if the primary beam electron density is very much less than the neutral particle density, which is the case for the system used by Koehler et al.[6] A lower bound on the secondary electron density can be obtained by equating the production rate, simply by stopping power of the relativistic electron beam to the loss rate given by dissociative recombination. This calculation yields a fractional ionization of the secondary plasma of approximately 1% (a lower bound). The actual value might be higher by a factor of 5 or 10. In summary, then, we estimate that the secondary plasma is hot and moderately ionized.

We believe that the major pumping of the gas [reaction (1)] is not achieved by collisions of the primary (relativistic) electrons with the xenon atoms, but by collisions of these hot secondary electrons with the xenon atoms. Our main justification for this assumption is that the excitation cross section for the production of xenon metastables [reaction (1)] seems to peak at an electron energy of ~40 eV and then rapidly fall off for higher electron energies. Therefore the excitation cross section is extremely small

for the high-energy primaries, whereas the hot secondaries are in a favorable energy range for direct population of the requisite xenon atom excited states. The ratio of primary electrons to secondaries is $\sim 10^{-7}$; therefore, if all other factors were equal (which we have shown they are not), then the electron pumping rate would be down by at least a factor of 10^{-7}. This can be seen in the following way. The pumping rate can be written as $n_e \langle Qv \rangle N_x$, where n_e is the electron density, $\langle Qv \rangle$ the velocity averaged cross section; that is,

$$\langle Qv \rangle = \int Qvf(v)\, d^3v,$$

where f(v) is the electron velocity distribution function, and N_x is the atom ground-state density. Therefore

$$\frac{P_{ump}(\text{primaries})}{P_{ump}(\text{secondaries})} = \frac{n_{ep} \langle Qv \rangle_p}{n_{es} \langle Qv \rangle_s}.$$

Recall that $\langle Qv \rangle_p \ll \langle Qv \rangle_s$ and that $n_{ep}/n_{es} \sim 10^{-7}$. Hence this ratio is $\ll 10^{-7}$.

We desire, therefore, to construct a plasma, at high pressures, which has hot electrons and is moderately ionized. Unfortunately, plasmas at high gas pressures tend to be highly ionized with moderately cool electrons, and these conditions are detrimental to the production of large metastable populations. If the plasma is highly ionized, the number of ground-state atoms present is low and, therefore, the excited dimer formation rate [reaction (6)] is very slow. The metastable destruction process [reaction (3)] involves cool electrons; therefore, if the electron-atom metastable collision frequency is greater than the atom-metastable-atom (three-body) rate, the desired metastables will be excited (or ionized) before they can react to form the excited dimer.

We shall now consider another method of obtaining large metastable atom densities in a cool, high-density plasma. Let us assume that somehow we can produce a highly ionized plasma that has cool electrons and cold gas atoms and ions. If these conditions are satisfied, then dissociative recombination will be the main plasma loss mechanism. We obtain the requisite atomic metastable population by the process of dissociative recombination [reaction (10)]. In our model the major share of the energy resides in ionization. This is illustrated by the potential-energy curves in Fig. XIV-2. Let us assume that some (or one) of the dissociative recombination paths (the repulsive curves that intercept the bound molecular ion state) which terminate on a manifold of atomic states are useful in producing $^3P_2$ atoms either directly or by cascades from high-lying states. Recall that if the electron energy is low, then spin exchange will be a fast process converting ^1P and ^3P states to $^3P_2$. For simplicity, we consider

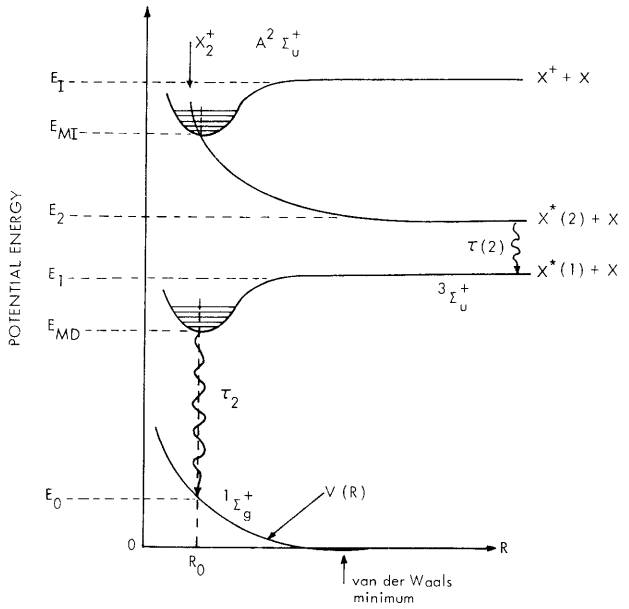

Fig. XIV-2. Potential energy curves for ground state, lowest excited dimer state, lowest bound ion dimer state, and a representative repulsive excited state, as a function of internuclear separation.

only two excited atomic states, the $^3P_2$ denoted $X^*(1)$ and some other higher lying state which is radiatively linked to the ^1P or ^3P states. We denote this state $X^*(2)$. For simplicity, we denote X_e by X.

We define the following coefficients which will soon be useful to us:

N_X = atomic ground-state density

n_e = electron density

X_2^+ = molecular ion density

X^+ = atomic ion density

α = dissociative recombination coefficient

α_c = collisional radiative recombination coefficient

β_+ = molecular ion formation coefficient

β = excited dimer formation coefficient

$X^*(1)$, $X^*(2)$, X_2^* = the excited state densities ($X^*(2) \rightarrow {}^3P_2$, and X_2^* represents the excited dimer density)

$\tau(2)$ = atomic radiative lifetime

τ_2 = molecular radiative lifetime.

Initially we assume that because of the large ground-state $\left({}^1S_o\right)$ density, radiation from the ${}^3P_1$ and ${}^1P_1$ states to the ${}^1S_o$ state is fully trapped. We do assume, however, that the radiation from the three-body collisional radiative recombination process escapes the plasma. We offer at this time no reason for this seeming contradiction except to note that compared with other energy-loss processes this (collisional recombination) loss is small. It provides a channel for electron loss from an initially hot, fully ionized plasma.

Neglecting Hornbeck-Molnar processes,[12] we have the following rate equations which describe the time evolution of the electron, ion, molecular ion, excited-state densities, electron temperature T_e and gas temperature T_g in the plasma afterglow.

Electrons (Afterglow)

$$\frac{\partial n_e}{\partial t} = -\left(a n_e X_2^+ + a_c n_e X^+\right) + \left(\underset{A\text{-}A}{\langle Qv \rangle} (X^*(2))^2 + \underset{A\text{-}A}{\langle Qv \rangle} (X^*(1))^2 \right.$$

$$\left. + \underset{M\text{-}M}{\langle Qv \rangle} \left(X_2^*\right)^2 \right) + n_e \left(\underset{e\text{-}A}{\langle Qv \rangle} X^*(2) + \underset{e\text{-}A}{\langle Qv \rangle} X^*(1) + \underset{e\text{-}M}{\langle Qv \rangle} X_2^* \right).$$

Here the second term in brackets on the right-hand side (for simplicity, we have neglected cross collision terms) represents the production of charged particles by excited-state processes [reactions (4) and (8)]. Early in the plasma afterglow these processes are also responsible for heating the electron gas. The third term on the right-hand side represents the production of charged particles by electron collisions with excited species [reaction (3)]. The later processes which are responsible for the major cooling of the electron gas have been estimated in the following manner. Recall that

$$\underset{e\text{-}A}{\langle Qv \rangle} = \int v \, \underset{e\text{-}A}{Q(v)} \, f(v) \, d^3v,$$

where f(v) is the electron-velocity distribution function. Since the early electron-electron rate is very large, we feel justified in taking for f(v) a Maxwellian. Recall that in an ionizing collision a certain amount of energy is required to remove an electron from an atom (dimer) and change it into a positive monovalent ion. For our case this minimum energy is the difference between the ionization energy and the energy of the excited state (E_1-E_2, see Fig. XIV-2). If the mean energy of the electrons is much smaller than the energy corresponding to the maximum of Q(v), denoted Q_m, we may approximate Q(v) in the following manner.[22]

$$Q = \sigma\left(v^2 - v_i^2\right)^{3/2}/v_i v \qquad v > v_i$$

$$= 0 \qquad v < v_i$$

where we have taken $1/2\ mv_i^2 = E_i$, the threshold energy. Averaging over a Maxwellian yields

$$\underset{e\text{-}A}{\langle Qv\rangle} = \frac{3\sigma}{v_i}\frac{kT_e}{m}\exp[-E_i/kT_e],$$

where for σ we have used the appropriate rates and cross sections listed above for xenon.

We consider the plasma to be singly ionized, that is, $n_e = X_2^+ + X^+$, so, because of this and the adherence of charge neutrality (the rare gases do not form negative ions if we ignore species analogous to the metastable $H_e(1s2s2p\ ^4P_{5/2})$), we need only one other charge continuity equation.

Molecular Ion

$$\frac{\partial X_2^+}{\partial t} = -\alpha n_e X_2^+ + \underset{M\text{-}M}{\langle Qv\rangle}\left(X_2^*\right)^2 + n_e\underset{e\text{-}M}{\langle Qv\rangle}X_2^* + \beta_+ N_x^2 X^+.$$

Excited States

$$\frac{\partial X^*(2)}{\partial t} = \alpha n_e X_2^+ - \frac{X^*(2)}{\tau(2)} - 2\underset{A\text{-}A}{\langle Qv\rangle}(X^*(2))^2 - n_e\underset{e\text{-}A}{\langle Q\text{-}v\rangle}X^*(2)$$

$$\frac{\partial X^*(1)}{\partial t} = \frac{X^*(2)}{\tau(2)} - \beta N_x^2 X^*(1) - 2\underset{A\text{-}A}{\langle Qv\rangle}(X^*(1))^2 - n_e\underset{e\text{-}A}{\langle Qv\rangle}X^*(1)$$

$$\frac{\partial X_2^*}{\partial t} = \beta N_x^2 X^*(1) - \frac{X_2^*}{\tau_2} - 2\underset{M\text{-}M}{\langle Qv\rangle}\left(X_2^*\right)^2 - n_e\underset{e\text{-}M}{\langle Qv\rangle}X_2^*.$$

These equations are written to conserve particles:

$$N_{x_o} = N_x + X^+ + X^*(2) + X^*(1) + 2X_2^+ + 2X_2^*,$$

where N_{x_o} is the "fill" particle density. For the cases of interest N_{x_o} is chosen so that

at all times $N_x \approx N_{x_o}$. This approximation, which simplifies the computations, introduces an error of ~5% at most.

We now must evaluate the electron and gas temperatures, taking $T_g = T_+$. In the equations above and in the energy-balance equations below we have assumed that the entire process is so fast that we may neglect the directed motion of the various particles. That is, we have neglected terms involving the spatial gradient ∇, such as the $\nabla \cdot (n\vec{v})$ term in the continuity equation. This greatly simplifies the mathematics, but may not be valid in a laser-produced plasma subject to violent shock waves. In this model spatial homogeneity is assumed.

Energy Balance[23] (T_e, T_g in eV)

$$\frac{\partial(N_x T_g)}{\partial t} = \frac{2m}{M}\,\nu_m n_e (T_e - T_g) + \left(\frac{2}{3}\right)\Big\{(E_I - E_{MI})\,\beta_+ N_x^2 X^+ + (E_1 - E_{MD})\,\beta N_x^2 X_2^* + (E_{MI} - E_2)\,\alpha n_e X_2^+ + E_o\left(X_2^*/\tau_2\right)\Big\} + n_e T_e\left(\alpha n_e X_2^+ + a_c n_e X^+\right).$$

$$\frac{\partial(n_e T_e)}{\partial t} = -\left(\frac{2m}{M}\right)\nu_m (T_e - T_g) + \frac{2}{3}\Big\{(2E_2 - E_I)\langle Qv\rangle_{A\text{-}A}\,(X^*(2))^2 + (2E_1 - E_I)\langle Qv\rangle_{A\text{-}A}\,(X^*(1))^2 + (2E_{MD} - E_{MI})\langle Qv\rangle_{M\text{-}M}\left(X_2^*\right)^2 - n_e\Big[(E_I - E_2)\langle Qv\rangle_{e\text{-}A}\,X^*(2) + (E_I - E_1)\langle Qv\rangle_{e\text{-}A}\,X^*(1) + (E_{MI} - E_{MD})\langle Qv\rangle_{M\text{-}M}\,X_2^*\Big]\Big\} - n_e T_e\left(\alpha n_e X_2^+ + a_c n_e X^+\right).$$

This set of nonlinear differential equations is numerically integrated on the IBM 370 computer. The computer code[24] makes use of a predictor-corrector method in conjunction with the partial derivatives of the rate equations with respect to the arguments (the partial derivative of $\partial n_e/\partial t$ with respect to n_e).

Plasma Initial Conditions

We define t = 0 as the time when the main plasma production via the applied electric field is turned off. Time thus represents time in the plasma afterglow.

At t = 0:

$n_e = 1.9 \times 10^{19}$ cm^{-3}	$N_x = 6.7 \times 10^{20}$ cm^{-3}
$T_e = 3.0$ eV	$T_g = 4 \times 10^{-2}$ eV
$E_I = 12.1$ eV	$E_{MI} = 12.0$ eV
$E_2 = 9.8$ eV	$E_1 = 8.3$ eV
$E_{MD} = 7.8$ eV	$E_o = 0.5$ eV
$\alpha_c = 10^{-10}$ cm^{-3} s^{-1}	$\tau(2) = 100$ ns
$X^*(2) = X^*(1) = X_2^+ = X_2^* = 0$	$\tau_2 = 50$ ns

The gas is xenon and all relevant data not listed in this report have been compiled by S. C. Brown.[8]

Figures XIV-3 and XIV-4 represent the computer output for these initial conditions.

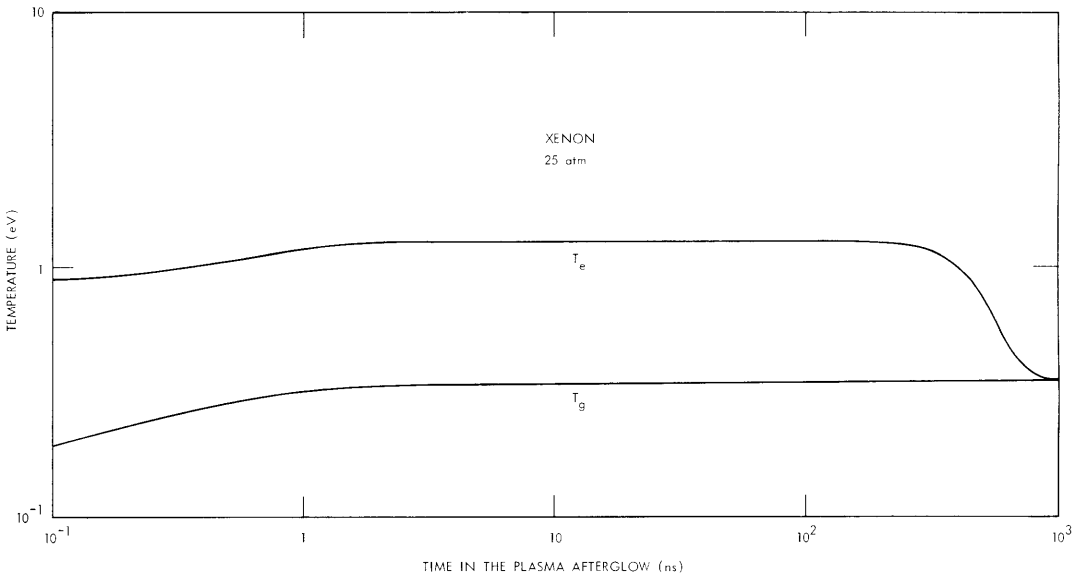

Fig. XIV-3. Electron and gas temperature as a function of time in the plasma afterglow. Initially (t = 0) $T_e = 3$ eV and $T_g = 4 \times 10^{-2}$ eV. We assume that $T_g = T_+ = T_{dimer}$.

In Fig. XIV-3 T_e and T_g are plotted as a function of time. Notice that T_e drops from its initial value (3 eV) to ~0.9 eV at t = 0.1 ns and then rises to ~1.25 eV because of excited-state collisional heating. The gas temperature continues to rise from its initial value primarily because of the dissociative recombination process. Since we have included no gas-cooling mechanism (heat conduction will not affect our result on this time scale) the gas temperature tends to saturate at ~0.34 eV.

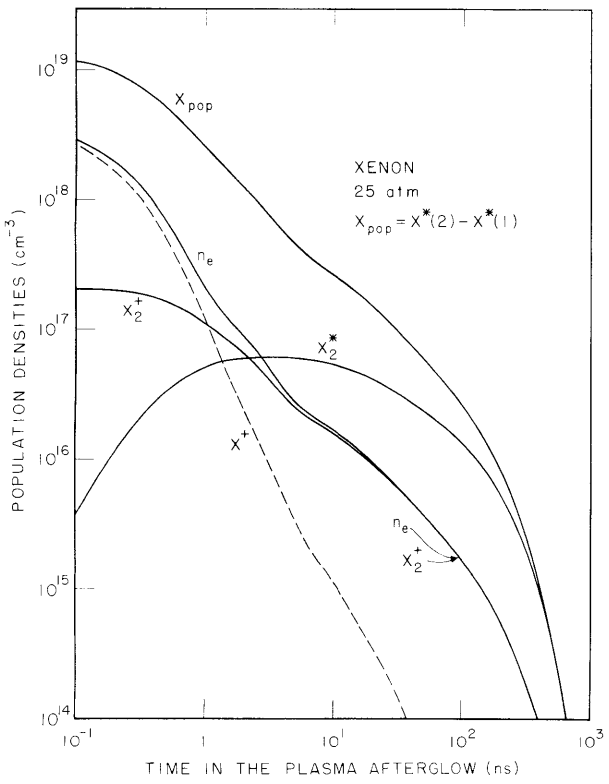

Fig. XIV-4.

Population densities as a function of time in the plasma afterglow. Initially $n_e = X^+ = 1.9 \times 10^{19}$ cm^{-3} and $X^*(2) = X^*(1) = X_2^+ = X_2^* = 0$. The model includes an electron temperature dependence on the electron-excited destruction process only.

Figure XIV-4 shows that n_e is maintained at a large value for some time because of the various plasma production terms that are operative. We see also that X_{pop}, defined as $X_{pop} = X^*(2) - X^*(1)$, peaks rapidly at ~$1.2 \times 10^{19}$ cm^{-3} (initially it was chosen equal to zero) and falls at a rate comparable to n_e which is to be expected. The excited dimer density X_2^* peaks at t ≈ 4 ns with a value of ~6×10^{16} cm^{-3}.

Notice that the potential radiative bottleneck, via $\tau(2)$, may be alleviated by designing the optical laser cavity so that it has mirrors of high reflectivity at both the ultraviolet wavelength and the wavelength that corresponds to the transition $X^*(2) \rightarrow X^*(1)$. If laser action then ensues, the spontaneous rate $\tau(2)$ is replaced by the faster stimulated rate. To see what effect laser action at the $X^*(2) \rightarrow X^*(1)$ transition has on the excited dimer density X_2^*, the computer code was rerun with the previously listed plasma initial conditions, except that $\tau(2)$ = 5 ns. Figure XIV-5 illustrates the time

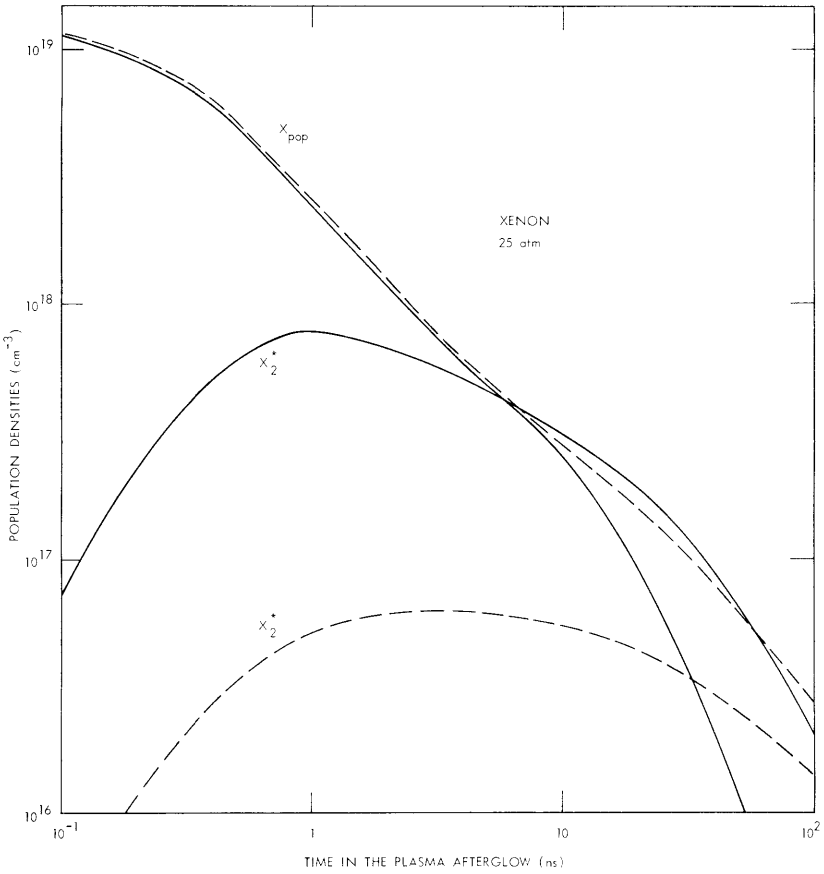

Fig. XIV-5. Excited dimer X_2^* and X_{pop} densities as a function of time in the plasma afterglow for two values of $\tau(2)$. The dashed line corresponds to $\tau(2)$ = 100 ns (same data as in Fig. XIV-4), and the solid line corresponds to $\tau(2)$ = 5 ns.

dependence of X_2^* and X_{pop} for both $\tau(2)$ = 100 ns (dashed lines) and $\tau(2)$ = 5 ns (solid lines). We see that if the transition $X^*(2) - X^*(1)$ lases, then the subsequent excited dimer density X_2^* is increased by more than one order of magnitude. This is to be expected, since in effect we have increased the rate of pumping to level $X^*(1)$.

In our simplified model we have neglected the temperature dependences on α. O'Malley[25] has derived a simple temperature dependence, valid for diatomic ions with large room-temperature recombination rates, of the form

$$\alpha = C\, T_e^{-1/2}(1-\exp[-h\nu/kT_g]).$$

In our next report we shall include gas and electron temperature dependences on the molecular formation rates. We are also investigating the magnitude of the electron heating as a result of superelastic collisions [reaction (13)].

It seems appropriate at this point to estimate the excited dimer density required to obtain laser action in an optical cavity, and to take into account losses from photoionization.

Estimate of Laser Gain

Let us assume that the active plasma is ~1 cm long and that the optical cavity losses are ~10%. To obtain laser action, the small-signal gain g_o should therefore exceed ~0.1 cm^{-1}. We shall take g_o to be ~1 cm^{-1} to allow for the photoionization loss which cannot be accurately estimated until X_2^* is known. Since the ground molecular state is virtually empty, we may write that at line center

$$g_o \approx X_2^* \frac{\omega_o}{\Delta\omega_o} \frac{|\mu_{uL}|^2}{\epsilon_o hc}.$$

Here $\Delta\omega_o$ is the bandwidth, and μ_{uL} is the appropriate dipole moment for the transition under study. Taking $(\omega_o/\Delta\omega_o) \sim 17$ and $\mu_{uL} \sim 10^{-29}$ Cm yields

$$X_2^* \gtrsim 1 \times 10^{17} \text{ cm}^{-3}.$$

The photoionization loss under these conditions is approximately 3×10^{-2} cm^{-1} and, therefore, is negligible compared with other losses. Although a more thorough theoretical analysis is warranted, this excited dimer density seems to be experimentally feasible.

References

1. The early work on continuous spectra was reviewed by W. Finkelnburg, Kontinuierliche Spektren (Springer Verlag, Berlin, 1938).
2. Y. Tanaka and M. Zelikoff, J. Opt. Soc. Am. 44, 254 (1954); P. G. Wilkinson and Y. Tanaka, J. Opt. Soc. Am. 45, 344 (1955); Y. Tanaka, J. Opt. Soc. Am. 45, 710 (1955).
3. (a) For He_2^* see M. L. Ginter and R. Battino, J. Chem. Phys. 52, 4469 (1970).

   (b) For Xe_2^* see R. S. Mulliken, J. Chem. Phys. 52, 5170 (1970).
4. R. S. Mulliken, J. Am. Chem. Soc. 86, 3183 (1964); R. S. Mulliken, J. Am. Chem. Soc. 88, 1849 (1966); R. S. Mulliken, J. Am. Chem. Soc. 91, 4615 (1969).
5. O. Cheshnovsky, B. Raz, and J. Jortner, Private communication relating to work performed in the Department of Chemistry at Tel-Aviv University. Also see J. Jortner et al., J. Chem. Phys. 42, 4250 (1965); and M. Martin, J. Chem. Phys. 54, 3289 (1971) for other data on the condensed phases.
6. H. A. Koehler, L. J. Ferderber, D. L. Redhead, and P. J. Ebert, Appl. Phys. Letters 21, 198 (1972).

7. B. Krawetz and C. K. Rhodes, "Vacuum Ultraviolet Studies of Rare Gases and Rare Gas Mixtures Excited with Pulsed High Energy Electron Beams," UCRL-73777, University of California (to be published).

8. S. C. Brown, Basic Data of Plasma Physics (The M. I. T. Press, Cambridge, Mass., 1968), p. 136.

9. Ibid., p. 143.

10. K. Wojaczek, Beitr. Plasma Phys. 5, 307 (1965), follows the classical method developed by M. Gryzinski. See, for example, M. Gryzinski, Phys. Rev. 115, 374 (1959).

11. A. V. Phelps and J. P. Molnar, Phys. Rev. 89, 1202 (1953). Also see H. S. W. Massey, Electronic and Ionic Impact Phenomena, Vol. 3, Slow Collisions of Heavy Particles (Oxford University Press, London, 1971).

12. J. A. Hornbeck and J. P. Molnar, Phys. Rev. 84, 621 (1951).

13. J. S. Dahler, J. L. Franklin, M. S. B. Munson, and F. H. Field, J. Chem. Phys. 36, 3332 (1962).

14. R. Boucique and P. Mortier, J. Phys. D 3, 1905 (1970). In this work there appears to be an inconsistency in the formation rate for krypton. If we model the interaction by a three-body van der Waals force, then the rate should scale roughly as the product of the polarizabilities and hence should increase with z. Three-body van der Waals forces are considered in H. Margenau and N. R. Kestner, Theory of Intermolecular Forces (Pergamon Press, New York, 2d ed., 1971); B. M. Axilrod and E. Teller, J. Chem. Phys. 11, 299 (1943).

15. For a recent compilation of these rates see E. W. McDaniel, V. Cermak, A. Dalgarno, E. E. Ferguson, and L. Friedman, Ion-Molecule Reactions (Wiley Interscience, New York, 1970).

16. T. R. Connor and M. A. Biondi, Phys. Rev. 140, A778-A791 (1965).

17. G. V. Marr, "Photoionization Processes in Gases," in Pure and Applied Physics, Vol. 28 (Academic Press, New York, 1967), p. 108.

18. H. J. Oskam and V. R. Mittelstadt, Phys. Rev. 132, 1445 (1963). For a recent discussion on dissociative recombination processes see the article by J. N. Bardsley and M. A. Biondi, in D. R. Bates (Ed.), Advances in Atomic and Molecular Physics, Vol. 6 (Academic Press, New York, 1970).

19. The atomic g-values of the low-lying atomic resonance lines of Kr and Xe are close to one another and near the j-j limit. See P. G. Wilkinson, Can. J. Phys. 45, 1709 (1967).

20. A. Gedanken, B. Raz, A. Szöke, and J. Jortner (to be published). Also reported by A. Szöke and B. Raz at the "Cambridge Conference on Molecular Energy Transfer, Cambridge, England, July 1971."

21. See, for example, E. W. McDaniel and M. R. C. McDowell, Case Studies in Atomic Collision Physics I (North-Holland Publishing Co., Amsterdam, 1969), Chap. 6. Also see W. K. Peterson, C. B. Opal, and E. C. Beaty, J. Phys. B 4, 1020 (1971).

22. T. Kihara, Rev. Mod. Phys. 24, 45 (1952).

23. I. P. Shkarofsky, T. W. Johnston, and M. P. Bachynski, The Particle Kinetics of Plasmas (Addison-Wesley Publishing Company, South Reading, Mass., 1966).

24. C. W. Gear, "Numerical Integration of Stiff Ordinary Differential Equations," Report No. 221, University of Illinois, 1967.

25. T. F. O'Malley, Phys. Rev. 185, 101 (1969).

B. PRODUCTION OF PLASMA BY LASER BREAKDOWN

Joint Services Electronics Programs (Contract DAAB07-71-C-0300)

C. W. Werner

For a more exact solution of the ion and atom densities discussed in Section XIV-A we must get a specific idea of the various initial conditions in the plasma afterglow. Consequently, we set up several models for the actual breakdown of the gas. Breakdown of the gas is initiated by the application of a strong electric field E. This field supplies a gain mechanism in the energy-balance equation for the electrons and supplies a mechanism for the ionization of the neutral gas atoms.

The energy-balance equation for the electrons is modified by the addition of the gain term

$$\frac{d}{dt}\frac{3}{2} n_e kT_e = n_e eEv_D - \text{loss mechanisms},$$

where v_D is the drift velocity of the electrons in the field. In terms of the mobility, this becomes

$$\frac{d}{dt}\frac{3}{2} n_e kT_e = n_e e\mu E^2 - \text{loss mechanisms}$$

$$= n_e \frac{e^2E^2}{m\nu_m} - \text{loss mechanisms}.$$

If we first assume that ionization and elastic recoil are the major loss mechanisms, this becomes

$$\frac{d\theta}{dt} = \frac{2}{3}\frac{e^2E^2}{m\nu_m} - \left(\nu_i + \frac{2m}{M}\nu_m\right)(\theta-\theta_g) - \frac{2}{3}\nu_l u_i,$$

where $\theta = kT_e$, $\theta_g = kT_{gas}$, ν_i = ionization frequency, ν_m = collision frequency for momentum transfer, and u_i = ionization potential. Here ν_i and ν_m are functions of the electron temperature, since

$$\nu_a = n_g \frac{\int_0^\infty vQ_a E^{1/2} e^{-E/\theta} dE}{\int_0^\infty E^{1/2} e^{-E/\theta} dE},$$

provided we assume a Maxwellian electron energy distribution. The cross sections

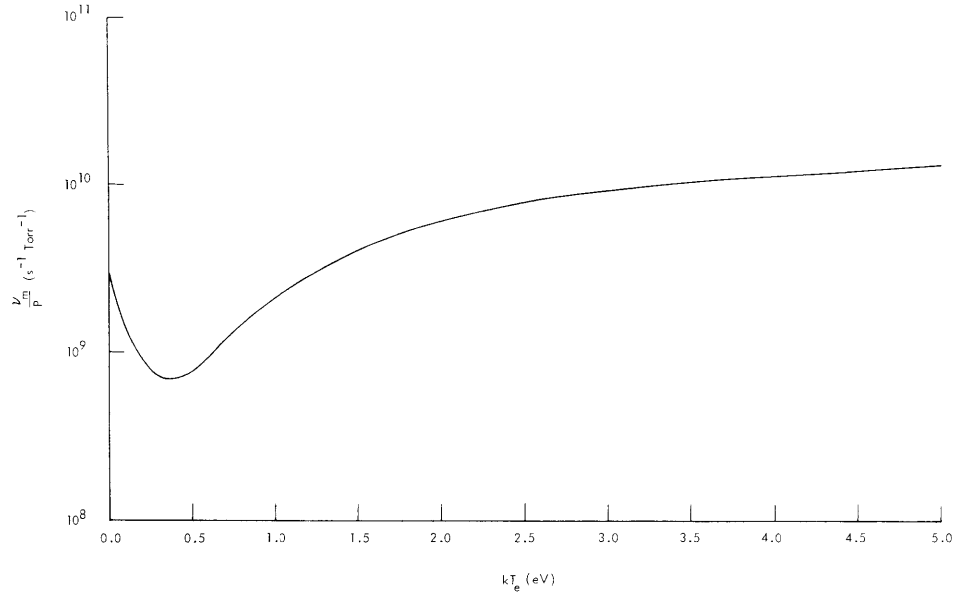

Fig. XIV-6. Collision frequency for momentum transfer in xenon vs electron temperature.

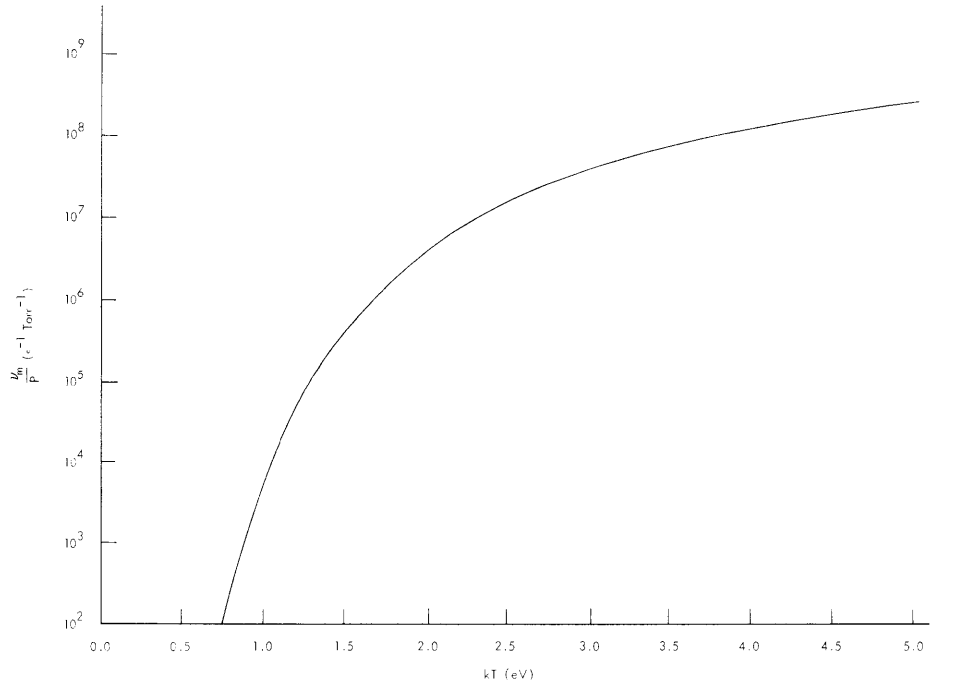

Fig. XIV-7. Ionization frequency in xenon vs electron temperature.

for ionization and for momentum transfer have been well tabulated.[1,2] It is a simple matter to integrate the equation above for various θ to get an expression for ν/p vs θ. This was done at intervals of approximately 0.1 eV (see Figs. XIV-6 and XIV-7).

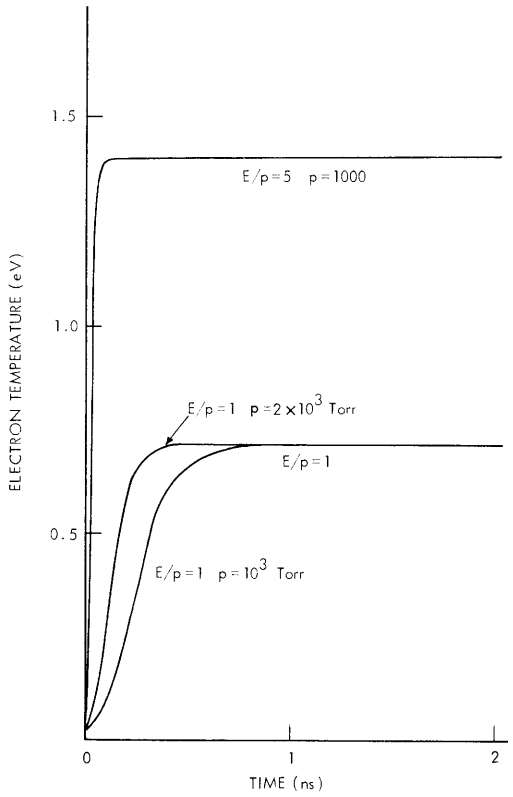

Fig. XIV-8. Electron temperature vs time for dc breakdown in xenon.

The energy balance equation can be solved by computer. Here, the data for ν_i and ν_m were supplied at intervals of 0.1 eV, and the computer was permitted to interpolate for points that were not given. In the dc case we see that the equilibrium electron temperature is a unique function of E/p, since in equilibrium

$$\frac{d\theta}{dt} = 0 = \frac{2}{3}\frac{e^2E^2}{m\nu_m^o p} - p\left(\nu_1^o + \frac{2m}{M}\nu_m\right)(\theta-\theta_g) - \frac{2}{3}p\nu_i^o u_i$$

$$\theta_{eq} = \theta_g + \frac{2}{3}\frac{\frac{e^2}{m\nu_m^o}\left(\frac{E}{p}\right)^2 - \nu_1^o u_i}{\nu_1^o + \frac{2m}{M}\nu_m^o}.$$

Furthermore, the characteristic time scales as 1/p for given E/p, as may be seen if we divide both sides of the energy-balance equation by p.

Similarly, the electron density as a function of time may be solved in a simple model if we assume that ionization is the major gain mechanism and recombination is the major loss mechanism. Thus $\frac{dn_e}{dt} = n_e \nu_i - \alpha n_e^2$, which leads to an equilibrium value of $n_e^{(eq)} = \frac{\nu_i}{\alpha}$. Again, ν_i is a function of the electron temperature, and this must be taken into account in the solution of equilibrium values.

Typical values for the temporal evolution of T_e are shown in Fig. XIV-8.

1. Laser Breakdown

In the case of laser breakdown, the expression for the field in the energy-balance equation must be modified. Microwave (ac) breakdown theory was used in this case. The field was modified for the ac case in the usual manner:[3]

$$E_{eff}^2 = E^2 \frac{\nu_m^2}{\nu_m^2 + \omega^2},$$

where ω is the angular frequency of the laser light used for breakdown. It is assumed that the light has a field $E = E^o e^{i\omega t}$.

If we assume that the laser beam is focused to an area of A cm^2, and that within the volume of breakdown the field is essentially constant, we may employ Poynting's vector to solve for E^2:

$$S = \frac{c}{4\pi} E^2,$$

where S = P/A, and

$$E^2 = \frac{4\pi P(t)}{Ac},$$

where P(t) is the power output of the laser. The energy-balance equation becomes

$$\frac{d\theta}{dt} = \frac{8\pi}{3} \frac{e^2}{mAc} \frac{p\nu_m}{p^2\nu_m^2 + \omega^2} P(t) - \text{loss}.$$

In this case, θ_{eq} is only a slowly varying function of E/p, since $\omega \gg p\nu_m$. Typical data are given in Fig. XIV-8 for a laser pulse of 10^8 W focused to an area of 0.1 cm^2. Here we assumed that the recombination coefficient was for molecular recombination,

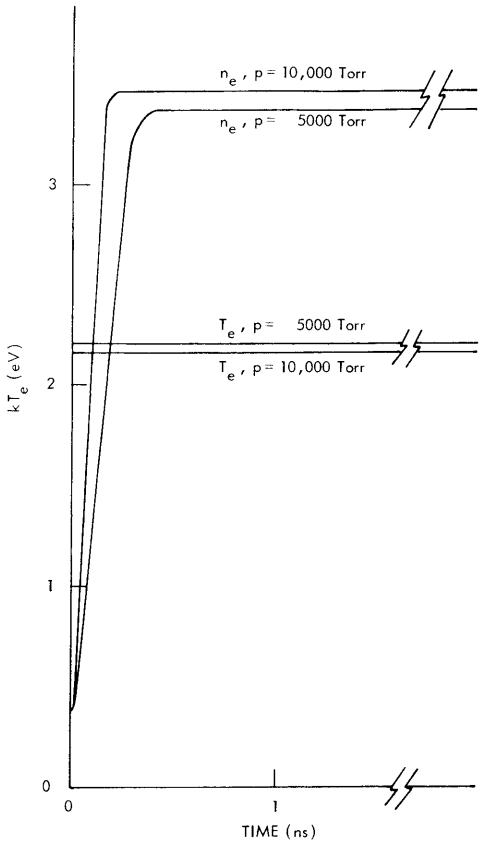

Fig. XIV-9.

Electron temperature and electron number density vs time for 10^8 W laser pulse breakdown. Area of focus is 0.1 cm^2.

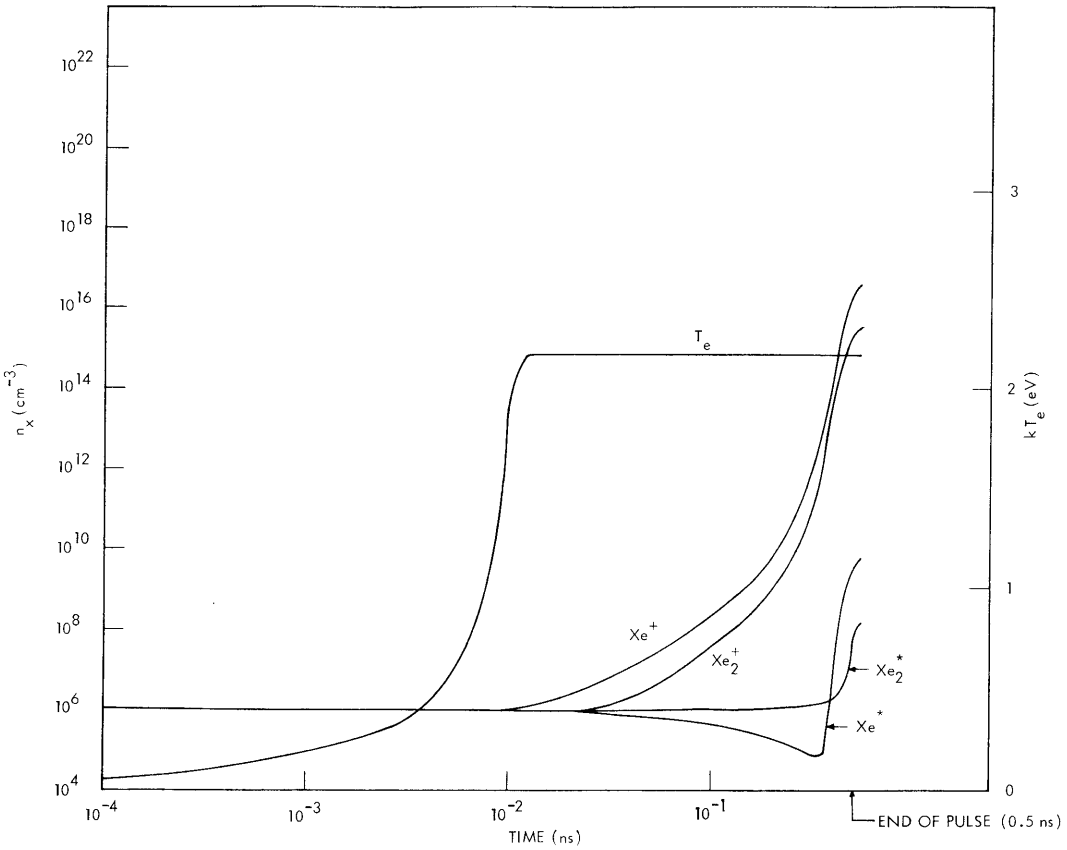

Fig. XIV-10.

Electron temperature and density for various molecular and ion species in xenon vs time. Laser power = 10^8 W. Pulse duration = 0.5 ns. Area of focus = 0.1 cm^2.

and did not depend on T_e. The equilibrium value of n_e is a lower bound, since the tacit assumption is that molecular recombination is the major source of loss. Since the recombination coefficient for atomic recombination

$$e + Xe^+ \rightarrow Xe$$

is approximately 4 orders of magnitude less, the value of n_e could be as much as 4 orders of magnitude greater. We shall take this into account in a later model.

A more complex model may now be assumed that takes into account most of the gain and loss mechanisms discussed by George and Rhodes in Section XIV-A. The solution of the equations for the temporal evolution of various ions and molecular species can also be accomplished by making reasonable estimates of cross-section data on the basis of the data discussed in Section XIV-A. Here we assumed that the cross sections were delta functions centered about the threshold energy of the process involved. Solution proceeds as before (see Fig. XIV-10). The data are for a 0.5 ns pulse.

As before, the electron temperature rapidly comes to equilibrium. The destructive effect of hot electrons on the Xe_2^* density (discussed in Section XIV-A) can be seen, although as the Xe_2^+ density climbs, this effect is apparently counteracted. The population is dominated, for the most part, by the atomic and molecular ions and, as predicted, the Xe_2^* densities remain very close to the initial value assumed. This confirms our suspicions that stimulated emission will be largely an afterglow phenomenon.

References

1. S. C. Brown, Basic Data of Plasma Physics (The M.I.T. Press, Cambridge, Mass., 1966), p. 136.
2. L. S. Frost and A. V. Phelps, Phys. Rev. 136, 1538 (1964).
3. S. C. Brown, Introduction to Electrical Discharges in Gases (John Wiley and Sons, Inc., New York, 1966), p. 166.